

Resolving gravitational redshift with sub-millimeter height differences using spin-squeezed optical clocks

Deshui Yu(于得水), Jia Zhang(张佳), Shougang Zhang(张首刚), Tiantian Shi(史田田), and Jingbiao Chen(陈景标)
Citation: Chin. Phys. B, 2025, 34 (**5**): 054208. DOI: 10.1088/1674-1056/adca1d
http://cpb.iphy.ac.cn; http://iopscience.iop.org/cpb

What follows is a list of articles you may be interested in

Electromagnetically-induced-absorption-like ground state cooling in a hybrid optomechanical system

Yaoyong Dong(董耀勇), Xuejun Zheng(郑学军), Denglong Wang(王登龙), and Peng Zhao(赵鹏)
Chin. Phys. B, 2025, 34 (**4**): 044203. DOI: 10.1088/1674-1056/adb260

Nonclassicality of photons in mean-field anisotropic quantum light-matter interacting lattices: Two-photon correlation function and quadrature squeezing

Xu-Min Chen(陈许敏), Pei-Yao Chen(陈佩瑶), and Chen Wang(王晨)
Chin. Phys. B, 2025, 34 (**4**): 044201. DOI: 10.1088/1674-1056/ada9db

Enhanced mechanical squeezing in an optomechanical system via backward stimulated Brillouin scattering

Shan-Shan Chen(陈珊珊), Yi-Long Xie(谢亦龙), Jing-Jing Zhang(张京京), Na-Na Zhang(张娜娜), Yong-Rui Guo(郭永瑞), Huan Yang(杨桓), and Yong Ma(马勇)
Chin. Phys. B, 2025, 34 (**1**): 014201. DOI: 10.1088/1674-1056/ad8cc0

Interrogation of optical Ramsey spectrum and stability study of an ^{87}Sr optical lattice clock

Jing-Jing Xia(夏京京), Xiao-Tong Lu(卢晓同), and Hong Chang(常宏)
Chin. Phys. B, 2022, 31 (**3**): 034209. DOI: 10.1088/1674-1056/ac11e0

Generation of atomic spin squeezing via quantum coherence: Heisenberg-Langevin approach

Xuping Shao(邵旭萍)
Chin. Phys. B, 2020, 29 (**12**): 124206. DOI: 10.1088/1674-1056/abab7c

---

RAPID COMMUNICATION

Resolving gravitational redshift with sub-millimeter height differences using spin-squeezed optical clocks

Deshui Yu(于得水)[1,2,†], Jia Zhang(张佳)[3,†], Shougang Zhang(张首刚)[1,2,4], Tiantian Shi(史田田)[5,6,‡], and Jingbiao Chen(陈景标)[3,7]

[1] *National Time Service Center, Chinese Academy of Sciences, Xi'an* 710600, *China*
[2] *Key Laboratory of Time Reference and Applications, Chinese Academy of Sciences, Xi'an* 710600, *China*
[3] *State Key Laboratory of Photonics and Communications, Institute of Quantum Electronics, School of Electronics, Peking University, Beijing* 100871, *China*
[4] *University of Chinese Academy of Sciences, Beijing* 100049, *China*
[5] *School of Integrated Circuits, Peking University, Beijing* 100871, *China*
[6] *National Key Laboratory of Advanced Micro and Nano Manufacture Technology, Beijing* 100871, *China*
[7] *Hefei National Laboratory, Hefei* 230088, *China*

(Received 5 March 2025; revised manuscript received 3 April 2025; accepted manuscript online 8 April 2025)

The phenomenon that a clock at a higher gravitational potential ticks faster than one at a lower potential, also known as gravitational redshift, is one of the classical tests of Einstein's theory of general relativity. Owing to their ultra-high accuracy and stability, state-of-the-art optical lattice clocks have enabled resolving the gravitational redshift with a millimeter-scale height difference. Further reducing the vertical inter-clock separation down to the sub-millimeter level and especially shortening the required measurement time may be achieved by employing spin squeezing. Here, we theoretically investigate the spin-squeezing-enhanced differential frequency comparison between two optical clocks within a lattice-trapped cloud of ^{171}Yb atoms. The numerical results illustrate that for a sample of 10^4 atoms, the atomic-collision-limited resolution of the vertical separation between two clocks can reach 0.48 mm, corresponding to a fractional gravitational redshift at the 10^{-20} level. In addition, the required averaging time may be reduced to less than one hundredth of that of conventional clocks with independent atoms. Our work opens a door to the future spin-squeezing-enhanced test of general relativity.

Keywords: optical lattice clock, quantum projection noise, spin squeezing, gravitational redshift

PACS: 42.50.–p, 42.62.Fi, 29.30.–h

DOI: 10.1088/1674-1056/adca1d **CSTR:** 32038.14.CPB.adca1d

1. Introduction

Einstein's theory of general relativity predicts that a clock (frequency ν_2) at a higher gravitational potential (height z_2) ticks faster than one (frequency ν_1) at a lower potential (height z_1),

$$\frac{\delta\nu_{\rm grs}}{\nu_1} = \frac{\nu_2-\nu_1}{\nu_1} = \frac{g}{c^2}(z_2-z_1) = (1.09\times10^{-16}\ {\rm m}^{-1})\times(z_2-z_1), \quad (1)$$

with the acceleration of gravity at the surface of Earth g and the speed of light c. This is known as gravitational redshift and was first observed on gamma rays in ground experiments in the 1960s.[1–3] Later, redshift measurements were performed through the frequency comparison between spaceborne and ground hydrogen masers with height differences of ten thousand kilometers.[4–6] Recently, more precise ground tests with height differences less than one kilometer have been performed on state-of-the-art optical lattice clocks (OLCs),[7–9] whose accuracy and stability have surpassed those of microwave counterparts by more than two orders of magnitude.[10]

We restrict ourselves to the detection of the gravitational redshift using OLCs whose systematic uncertainty limits the resolution, i.e., the minimum resolvable height difference between two clocks. The main sources of uncertainty of OLCs arise from lattice-induced light shifts, black-body radiation (BBR) shifts, and collisional (density) frequency shifts of clock-transition lines. Careful measurement of the electric-quadrupole and magnetic-dipole polarizabilities and the hyperpolarizability in atoms that are under interrogation allows for suppressing the uncertainty of light shifts down to the 10^{-19} level.[11,12] The fractional uncertainty of BBR shift can be controlled at the 10^{-18} level by utilizing *in situ* monitoring the ambient temperature[10] or directly placing OLCs in cryogenic environments.[13] Engineering the interactions between spin–orbit-coupled atoms potentially eliminates the density shift.[14] These advances have enabled resolving the gravitational redshift for millimeter-scale difference in height[15] and also constrained the violation from Einstein's theory of gen-

[†]These authors contributed equally to this work.
[‡]Corresponding author. E-mail: tts@pku.edu.cn
© 2025 Chinese Physical Society and IOP Publishing Ltd. All rights, including for text and data mining, AI training, and similar technologies, are reserved.

eral relativity down to the 10^{-5} level, the best constraint on the gravitational redshift on the ground.[9]

The stability of OLCs determines the statistical uncertainty of the clock comparison, which limits the required sampling time τ for resolving a tiny frequency shift. The main noise source degrading the clock stability is the so-called Dick effect, which originates from the aliasing of laser frequency noise due to the non-continuous interrogation of atoms.[16] Nevertheless, measuring the absolute frequency of a clock is unnecessary in some practical applications. Thus, employing the differential frequency comparison, where two (sub-)ensembles of atoms are quasi-simultaneously interrogated by a clock laser, can effectively reject the laser noise, leading to a QPN (quantum projection noise)-limited stability[17]

$$\sigma_y(\tau) = \frac{\Delta\phi}{2\pi\nu T_{\rm dark}}\sqrt{\frac{T_{\rm cyc}}{\tau}}, \tag{2}$$

with the phase uncertainty of Ramsey spectroscopy $\Delta\phi$, the Ramsey dark time $T_{\rm dark}$, and the clock cycle duration $T_{\rm cyc}$. Additionally, instead of the relatively short atom–light coherence time, the clock interrogation time in the differential frequency comparison is primarily determined by the atom–atom coherence time, which can be up to tens of seconds for atoms trapped in a shallow lattice.[15] The enhanced duty cycle is particularly beneficial for achieving a stability at the $10^{-18}/\sqrt{\tau}$ level, that is, suppressing the statistical uncertainty to the 10^{-21} level after about one hundred hours of averaging.

Conventional OLCs employ N independent (uncorrelated) atoms. Within each clock cycle, the light pulse from the local oscillator (clock laser) brings the ensemble into a coherent spin state (CSS) and the phase difference between the clock laser and the reference transition in atoms is read out through the projection measurement (i.e., projecting all atoms from the CSS into one clock state). In the absence of technical noise sources, the phase sensitivity (i.e., minimum resolvable phase difference) in Eq. (2) is limited by the QPN, $(\Delta\phi)_{\rm CSS} = N^{-0.5}$.[18,19] A large atom number (for example, $N \sim 10^5$ in Ref. [15]) is essential to substantially suppress the QPN, which, however, inevitably enhances the systematic uncertainty related to the atomic density. It has been recognized that the QPN limit may be overcome by preparing atoms in spin-squeezed states (SSSs),[20] resulting in a phase uncertainty $(\Delta\phi)_{\rm SSS} = N^{-\chi}$ with $\chi > 0.5$. Indeed, the fundamental bound on the measurement precision is imposed by the Heisenberg limit with $\chi = 1$.

For a given statistical uncertainty, the spin-squeezing-induced metrological gain leads to a reduction of the averaging time τ by a factor of $N^{(2\chi-1)}$. In theory, unconditional spin squeezing in the one-axis twisting (OAT) model yields $\chi \sim 5/6$,[21,22] according to which the measurement precision at the 10^{-21} level in Ref. [15] is potentially achieved within $\tau = 3$ minutes, corresponding to $N^{(2\chi-1)} = 2000$. A recent proof-of-principle experiment has achieved the OAT-spin-squeezed ^{171}Yb OLC with the ultra-narrow optical $6s^2\ {}^1S_0$–$6s6p\ {}^3P_0$ clock transition (wavelength of 579 nm and frequency of 518 THz).[23] The $6s^2\ {}^1S_0$–$6s6p\ {}^3P_1$ transition (wavelength of 556 nm) in ^{171}Yb is coupled to an optical cavity so as to provide the cavity-mediated coherent feedback, creating unconditional spin squeezing.[24] The reported metrological gain reached 5.7 dB over the QPN.[23] More recently, conditional spin squeezing has been performed on the state-of-the-art ^{87}Sr OLC with the $5s^2\ {}^1S_0$–$5s5p\ {}^3P_0$ clock transition (wavelength of 698 nm and frequency of 429 THz) by means of cavity quantum electrodynamics (cavity QED).[25,26] Spin ensembles experienced successive quantum non-demolition measurements and conditional spin squeezing was created for the joint measurement of the collective spin population inversion. The measurement precision of the differential frequency comparison of two clocks reached 7.3×10^{-17} at 300 s of averaging.[25,26]

In this paper, we numerically explore resolving the gravitational redshift through the differential frequency comparison between two spin-squeezed optical clocks that are located in one lattice-trapped atomic cloud. Under the assumption that the two clocks experience the same environmental conditions such as lattice-induced light shifts and ambient temperature fluctuations, the atom–atom collisions primarily disturb the clock comparison measurement. For a typical atom number of 10^4, the resolution of the fractional gravitational redshift is found to be 5.2×10^{-20}, corresponding to a sub-millimeter (0.48 mm) height difference between two clocks. Further, compared to the QPN-limited clock comparison, the required averaging time for sufficiently suppressing the statistical uncertainty is shortened by a factor of $\sim 10^2$ using spin squeezing. This study prefigures the necessary correction for gravitational perturbations in the future ultra-low uncertainty clock operation.

2. Results

2.1. Physical model

For the differential frequency comparison of two clocks within one atomic cloud, the clocks experience the same light shift noise and ambient temperature fluctuations. Our aim is to figure out the minimum cloud size for resolving the gravitational redshift in the presence of atom–atom collisions.

Let us focus on a general scheme of differential frequency comparison as shown in Fig. 1. N Fermi atoms are trapped in a one-dimensional optical lattice that is formed inside an optical cavity (lattice cavity). The optical lattice is oriented along the z axis (opposite to the gravitational acceleration g). Each atom is modeled as a spin-1/2 particle composed of upper $|\uparrow\rangle$

and lower $|\downarrow\rangle$ states with an energy difference $h\nu$ (h is Planck's constant). The optical lattice is operated at a magic wavelength $\lambda_{\rm mag}$ for the clock $|\downarrow\rangle$–$|\uparrow\rangle$ transition. The motional state populated by an atom is labeled by the vector $\boldsymbol{m} = (m_x, m_y, m)$, where the radial index $m_{u=x,y} = 0, 1, 2, \ldots$ corresponds to the harmonic oscillator $\phi_{m_u}(u)$ in the u axis and $m = 0, \pm1, \pm2, \ldots$ denotes the Wannier–Stark state $W_m(z)$ localized on the mth lattice site.[27,28] The law of conservation of atom number requires $\sum_{\boldsymbol{m}} 1 = N$. In practice, the number of lattice-trapped atoms N varies each time when a new atomic cloud is prepared. For an average atom number $\bar{N} \sim 10^3$, the standard deviation σ_N of N can be controlled to the level of 1% in experiments.[17]

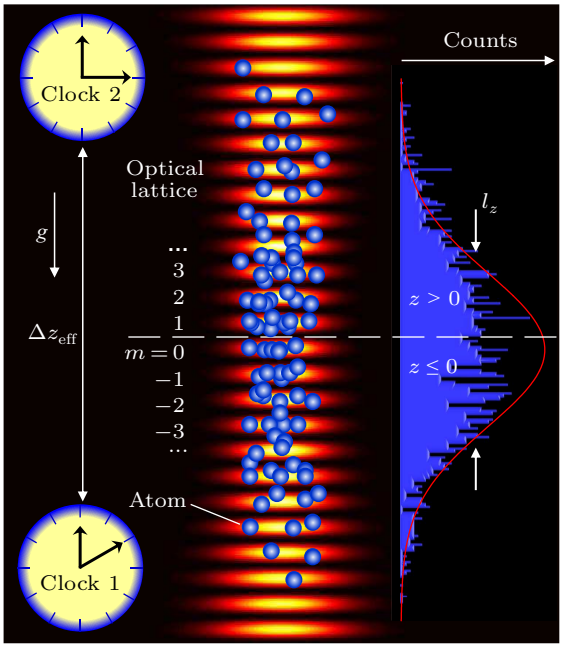


Fig. 1. Differential frequency comparison between two optical clocks within an ensemble of atoms. The lattice-trapped atoms present a Gaussian distribution along the gravity direction (acceleration of gravity g). The full width at half maximum of the atomic cloud along the lattice axis is l_z. Clock 1 (2) contains the atoms on the lattice sites with the indices $m \le 0$ ($m > 0$).

In the z axis, the atomic cloud follows a Gaussian density distribution with a full width at half maximum (FWHM) l_z. The average number of atoms on the mth lattice site is evaluated to be

$$\bar{n}_m = \sum_{\boldsymbol{m}' \ \&\ m'=m} 1 = \frac{N\sqrt{\ln 2}}{(l_z/\lambda_{\rm mag})\sqrt{\pi}} \mathrm{e}^{-\left(m\lambda_{\rm mag}\sqrt{\ln 2}/l_z\right)^2}. \quad (3)$$

Here, we have assumed that the atoms are maximally localized on the $m = 0$ site. Following the idea of synchronous Ramsey spectroscopy,[15,29] we divide the atomic cloud into two groups: clock 1 composed of atoms with $m \le 0$ and clock 2 with $m > 0$. Since the atoms on the $m = 0$ lattice site are included in clock 1, the average number of atoms in clock 1 slightly exceeds that of clock 2. The gravitational redshift $\delta\nu_{\rm grs}$ is derived from the differential frequency comparison between the two clocks. The average value of $\delta\nu_{\rm grs}$ is computed to be

$$\begin{aligned} \frac{\overline{\delta\nu}_{\rm grs}}{\nu} &= \frac{2g}{c^2}\sum_{m=1}^{\infty}\frac{n_m}{N}\frac{m\lambda_{\rm mag}}{2} \\ &= \frac{g}{c^2}\frac{l_z}{\sqrt{4\pi\ln 2}} = (3.70\times10^{-17}\ \mathrm{m}^{-1})\times l_z. \end{aligned} \quad (4)$$

It is seen that the atoms on the $m = 0$ lattice site do not contribute to $\overline{\delta\nu}_{\rm grs}$. In practice, the number of atoms on the mth lattice site fluctuates around $\bar{n}_m$, leading to a deviation $\sigma(\delta\nu_{\rm grs})$ of $\delta\nu_{\rm grs}$. Comparing Eq. (4) with Eq. (1), one obtains the effective height difference between the effective centers of mass of two clocks

$$\Delta z_{\rm eff} \approx 0.34 \times l_z, \quad (5)$$

which reaches 1 mm when $l_z = 2.9$ mm.

2.2. Atom–atom collisions

We assume that two clocks situated in the same optical lattice are exposed to the same environmental conditions. The differential clock comparison rejects technical noise such as lattice-induced light shifts and ambient temperature fluctuations. The remaining major source of noise originates from the atom–atom collisions.

To formulate interatomic interactions, we define the spin operator associated with the atom labeled by $\boldsymbol{m}$ as $\hat{\boldsymbol{s}}_{\boldsymbol{m}} = \sum_{u=x,y,z}\hat{s}^u_{\boldsymbol{m}}\boldsymbol{e}_u$ with three components $\hat{s}^x_{\boldsymbol{m}} = [(|\uparrow\rangle\langle\downarrow|)_{\boldsymbol{m}} + (|\downarrow\rangle\langle\uparrow|)_{\boldsymbol{m}}]/2$, $\hat{s}^y_{\boldsymbol{m}} = \mathrm{i}[(|\downarrow\rangle\langle\uparrow|)_{\boldsymbol{m}} - (|\uparrow\rangle\langle\downarrow|)_{\boldsymbol{m}}]/2$, and $\hat{s}^z_{\boldsymbol{m}} = [(|\uparrow\rangle\langle\uparrow|)_{\boldsymbol{m}} - (|\downarrow\rangle\langle\downarrow|)_{\boldsymbol{m}}]/2$. Adding spin operators of individual atoms in clock $i = 1, 2$ yields the total spin $\hat{\boldsymbol{S}} = \sum_{\boldsymbol{m}}\hat{\boldsymbol{s}}_{\boldsymbol{m}}$ of clock i. Under the condition of initially preparing all atoms in $|\downarrow\rangle$, i.e., the spin-polarized ensemble, the Hilbert space of clock i may be spanned by the maximally symmetric Dicke states $\{|S, M\rangle, M = -S, (-S+1), \ldots, (S-1), S\}$ with the total angular momentum $S = N_i/2$ and the projection M. Here, N_i denotes the number of atoms in clock i. The all-spin-down (all-spin-up) state is given by $|S, -S\rangle = \Pi_{\boldsymbol{m}} \otimes |\downarrow\rangle_{\boldsymbol{m}}$ ($|S, S\rangle = \Pi_{\boldsymbol{m}} \otimes |\uparrow\rangle_{\boldsymbol{m}}$).

Following the many-body spin model in Ref. [14], the atom–atom interactions including s- and p-wave scattering in clock $i = 1, 2$ are governed by the operator

$$\begin{aligned} \hat{V} = \sum\nolimits_{\boldsymbol{m}\neq\boldsymbol{m}'} \big[&\kappa_{\boldsymbol{m}\boldsymbol{m}'}\hat{\boldsymbol{s}}_{\boldsymbol{m}}\cdot\hat{\boldsymbol{s}}_{\boldsymbol{m}'} + \chi_{\boldsymbol{m}\boldsymbol{m}'}\hat{s}^z_{\boldsymbol{m}}\hat{s}^z_{\boldsymbol{m}'} \\ &+\gamma_{\boldsymbol{m}\boldsymbol{m}'}\left(\hat{s}^z_{\boldsymbol{m}} + \hat{s}^z_{\boldsymbol{m}'}\right)\big], \end{aligned} \quad (6)$$

with $\kappa_{\boldsymbol{m}\boldsymbol{m}'} = B^{(\uparrow\downarrow)}_{\boldsymbol{m}\boldsymbol{m}'} - A_{\boldsymbol{m}\boldsymbol{m}'}$, $\chi_{\boldsymbol{m}\boldsymbol{m}'} = B^{(\uparrow\uparrow)}_{\boldsymbol{m}\boldsymbol{m}'} + B^{(\downarrow\downarrow)}_{\boldsymbol{m}\boldsymbol{m}'} - 2B^{(\uparrow\downarrow)}_{\boldsymbol{m}\boldsymbol{m}'}$, and $2\gamma_{\boldsymbol{m}\boldsymbol{m}'} = B^{(\uparrow\uparrow)}_{\boldsymbol{m}\boldsymbol{m}'} - B^{(\downarrow\downarrow)}_{\boldsymbol{m}\boldsymbol{m}'}$. The s- and p-wave interaction strengths are respectively derived as $A_{\boldsymbol{m}\boldsymbol{m}'} = (2ha/m_{\rm a})\xi_{m_x m'_x}\xi_{m_y m'_y}\rho_{mm'}$ and $B^{(\alpha\beta)}_{\boldsymbol{m}\boldsymbol{m}'} = (3h^2 b^3_{\alpha\beta}/8\pi m_{\rm a})(\xi_{m_x m'_x}\eta_{m_y m'_y} + \eta_{m_x m'_x}\xi_{m_y m'_y})\rho_{mm'}$ with the s-wave scattering length a, the p-wave scattering volumes $b^3_{\alpha\beta}$

$(\alpha,\beta=\uparrow,\downarrow)$, the mass of atom $m_{\rm a}$, the overlap integrals between transverse spatial modes of atoms

$$\xi_{m_u m'_u}=\int|\phi_{m_u}(u)\phi_{m'_u}(u)|^2\,{\rm d}u, \tag{7a}$$

$$\eta_{m_u m'_u}=\int|\phi_{m_u}(u)\partial_u\phi_{m'_u}(u)-\phi_{m'_u}(u)\partial_u\phi_{m_u}(u)|^2\,{\rm d}u, \tag{7b}$$

with $u=x,y$, and the overlap integrals between Wannier–Stark states

$$\rho_{mm'}=\int|W_m(z)W_{m'}(z)|^2\,{\rm d}z. \tag{8}$$

Each $\boldsymbol{m}$ state in the summation of Eq. (6) is populated by one atom. Since each clock cycle starts with the spin-polarized ensemble, the Fermi–Dirac statistics forbids s-wave interactions between atoms on different lattice sites. As a result, the on-site p-wave interactions with $m=m'$ dominate the collisional shifts.

We employ Ramsey spectroscopy to measure the frequency shift of clock $i=1,2$. The atom–atom collisions mainly occur within the dark period (duration $T_{\rm dark}$), during which the state of atoms evolves according to

$$\frac{{\rm i}h}{2\pi}\frac{\rm d}{{\rm d}t}\psi(t)=\hat{V}\psi(t). \tag{9}$$

Solving the above Schrödinger equation needs the following transition matrix elements:

$$\begin{aligned}&\langle S,M'|\,(\hat{s}^{\rm x}_{\boldsymbol{m}}\pm{\rm i}\hat{s}^{\rm y}_{\boldsymbol{m}})\,|S,M\rangle\\&=\frac{\sqrt{(S\pm M+1)(S\mp M)}}{2S}\delta_{M',M\pm1},\end{aligned} \tag{10a}$$

$$\langle S,M'|\,\hat{s}^{\rm z}_{\boldsymbol{m}}\,|S,M\rangle=\frac{M}{2S}\delta_{M',M}, \tag{10b}$$

on the basis of Dicke states. The interaction operator $\hat{V}$ introduces an extra phase shift to each $|S,M\rangle$ after the free evolution time and all these phases eventually lead to a collisional shift in the Ramsey measurement.

2.3. Spin squeezing

In the Ramsey measurement, the clock phase is usually read out by projecting all atoms into, for example, $|\uparrow\rangle$. The QPN primarily limits the detection sensitivity for independent atoms. It has been demonstrated that the QPN limit can be overcome using spin squeezing.[23,25,26] The enhanced clock stability strongly shortens the minimum averaging time that is necessary for resolving a tiny frequency shift. In order to maximize the spin-squeezing-induced metrological gain in the differential clock comparison, the atoms in individual clocks in Fig. 1 are prepared in SSSs while the two clocks are uncorrelated with each other.[30] In the specific implementation of spin squeezing, the atomic cloud is situated inside an extra optical cavity that intersects the optical lattice. This perpendicular cavity is driven by a squeezing laser to provide coherent quantum feedback, consequently suppressing the quantum fluctuations of atoms.[24] Addressing two independent spin-squeezed clocks can be carried out by means of the moving optical lattice as experimentally demonstrated in Ref. [25]. Detuning one lattice beam transports two sub-ensembles (clocks) into and out of the perpendicular cavity successively, creating spin squeezing of individual clocks.

Here, we utilize the OAT model to implement spin squeezing as shown in Fig. 2(a). The specific approach can be summarized as follows: All spins in clock $i=1,2$ are initially prepared in the spin-down state $|S,-S\rangle$. The first Ramsey $\pi/2$-pulse brings the sub-ensemble into

$$|{\rm CSS}\rangle={\rm e}^{-{\rm i}\pi\hat{S}_x/2}\,|S,-S\rangle=\Pi_{\boldsymbol{m}}\otimes(|\downarrow\rangle_{\boldsymbol{m}}-{\rm i}\,|\uparrow\rangle_{\boldsymbol{m}})/\sqrt{2}. \tag{11}$$

Then, the sub-ensemble evolves according to the OAT evolution operator, $\hat{O}_{\rm OAT}(\alpha)={\rm e}^{-{\rm i}(\pi+\alpha)\hat{J}_z^2}$ with an angle α. Subsequently, the rotation operation around the y-axis is performed, $\hat{O}_{\rm R}(\beta)={\rm e}^{-{\rm i}(\pi/2+\beta)\hat{J}_y}$ with an angle β, and the sub-ensemble state arrives at

$$|{\rm SSS}\rangle=\hat{O}_{\rm R}(\beta)\hat{O}_{\rm OAT}(\alpha)\,|{\rm CSS}\rangle\,. \tag{12}$$

Later, the atoms experience a dark period (duration $T_{\rm dark}$), during which the atom–atom interactions take the main effects [see Eq. (6)]. After the second Ramsey $\pi/2$-pulse, one obtains

$$|\psi\rangle\propto{\rm e}^{-{\rm i}\pi\hat{S}_x/2}\,{\rm e}^{-{\rm i}2\pi\hat{V}T_{\rm dark}/h}\,|{\rm SSS}\rangle\,. \tag{13}$$

Performing the projection measurement on $|\psi\rangle$ gives the fractional excitation

$$p=1/2+\langle\psi|\,\hat{S}_z\,|\psi\rangle/N, \tag{14}$$

and the clock phase reads $\phi=p-1/2$. The phase detection sensitivity is given by

$$\Delta\phi=\Delta p/|\partial_\phi p|, \tag{15}$$

with the measurement deviation

$$\Delta p=\sqrt{\langle\psi|\,\hat{S}_z^2\,|\psi\rangle-\langle\psi|\,\hat{S}_z\,|\psi\rangle^2}/N.$$

In the absence of atom–atom interactions ($\hat{V}=0$), the phase uncertainty of clocks with independent atoms ($\hat{O}_{\rm R}=\hat{O}_{\rm OAT}=\hat{I}$ with the unit operator $\hat{I}$) corresponds to the QPN limit, $(\Delta\phi)_{\rm CSS}=N^{-0.5}$. By contrast, the phase uncertainty of spin-squeezed clocks can be lower than that of CSS, i.e., $(\Delta\phi)_{\rm SSS,0}/(\Delta\phi)_{\rm CSS}<1$ (Fig. 2(b)). Here, the subscript "0" denotes the absence of interatomic interactions $\hat{V}=0$. We numerically determine the optimal angles (α,β) that minimize $(\Delta\phi)_{\rm SSS,0}$ and find the scaling $\alpha\propto N^{-0.642}$ and $\beta\propto N^{-0.358}$ (Fig. 2(c)), resulting in the ratio $(\Delta\phi)_{\rm SSS,0}/(\Delta\phi)_{\rm CSS}\propto N^{-0.356}$ (Fig. 2(d)). Our numerical results are close to the analytical

solutions $\alpha \propto N^{-2/3}$, $\beta \propto N^{-1/3}$, and $(\Delta\phi)_{\mathrm{SSS},0}/(\Delta\phi)_{\mathrm{CSS}} \sim N^{-1/3}$ derived in Refs. [21,22] in the limit of $N \to \infty$. The SSS of $N = 5000$ atoms gives $(\Delta\phi)_{\mathrm{SSS},0}/(\Delta\phi)_{\mathrm{CSS}} = 0.062$, which corresponds to a sensitivity enhancement decibel value of 12 dB. Nevertheless, as we will see below, the presence of atom–atom interactions ($\hat{V} \neq 0$) introduces extra phases to the SSS [see Eq. (13)], leading to a degradation of spin squeezing $(\Delta\phi)_{\mathrm{SSS}} > (\Delta\phi)_{\mathrm{SSS},0}$.

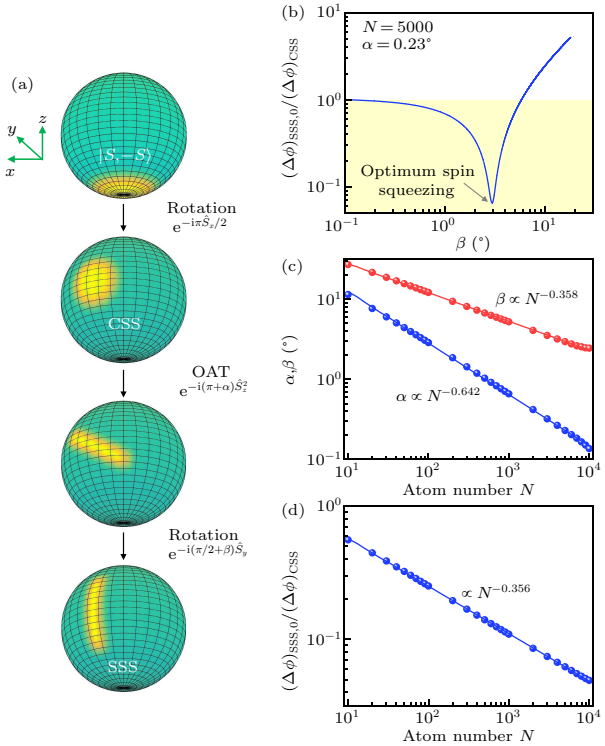


Fig. 2. Spin squeezing. (a) Evolution of the spin state on the Bloch sphere. The first Ramsey $\pi/2$-pulse, the one-axis twisting, and the rotation operation around the y-axis are performed subsequently on the initial state $|S,-S\rangle$. (b) The phase uncertainty $(\Delta\phi)_{\mathrm{SSS}}$ in the SSS-based Ramsey detection as a function of the rotation angle β with the atom number $N = 5000$ and the angle $\alpha = 0.23°$. (c) Dependence of the optimal pair (α,β) on the atom number N. Symbols: numerical results. Lines: curve fitting, $\log_{10}\alpha = 1.738 - 0.642\log_{10}N$ and $\log_{10}\beta = 1.80 - 0.358\log_{10}N$. (d) Ratio $(\Delta\phi)_{\mathrm{SSS},0}/(\Delta\phi)_{\mathrm{CSS}}$ as a function of N. Symbols: numerical results. Line: curve fitting, $\log_{10}[(\Delta\phi)_{\mathrm{SSS},0}/(\Delta\phi)_{\mathrm{CSS}}] = 0.109 - 0.356\log_{10}N$.

2.4. Shallow-lattice ytterbium clocks

We restrict ourselves to ^{171}Yb OLCs since OAT spin squeezing has been recently demonstrated on the $|\downarrow\rangle = 6s^2\ {}^1S_0(F = 1/2, M_F = -1/2) - |\uparrow\rangle = 6s6p\ {}^3P_0(F = 1/2, M_F = -1/2)$ clock transition ($\nu = 518$ THz and $\lambda_{\mathrm{mag}} = 759$ nm) in neutral ytterbium.[23] Here, F denotes the total angular momentum and M_F corresponds to the z-projection. In the conventional clock operation, the lattice depth U reaches up to hundreds of the photon recoil energy $E_{\mathrm{rec}} = h^2/2m_a\lambda_{\mathrm{mag}}^2 = 97.2$ nK. The enhanced Raman scattering of lattice photons by atoms shortens the lifetime of $|\uparrow\rangle$ to less than 1 s,[31,32] although the natural linewidth of the clock transition approximates 10 mHz.[33] Operating the clock in a shallow lattice may extend the lifetime of $|\uparrow\rangle$ over 10 s.[34,35]

In what follows, we choose $U = 10E_{\mathrm{rec}}$ (i.e., shallow optical lattice), assume the Ramsey dark time $T_{\mathrm{dark}} = 1$ s, and neglect the effects of the lattice photon scattering on the clock operation. On each lattice site, the atoms are prepared in the lowest Wannier–Stark state of the axial motion. The oscillation frequency of the radial motion of atoms is evaluated as $\nu_r = (2\pi w)^{-1}\sqrt{4U/m_a} = 22$ Hz with the lattice beam waist $w = 100$ μm. In the shallow optical lattice, the radial atomic temperature T_r should be reduced accordingly. Otherwise, the atoms cannot be effectively trapped. Here, we assume $T_r = 200$ nK, which is experimentally feasible under the current experimental conditions.[14,36,37] The resultant average occupation of vibrational states reaches $k_B T_r/h\nu_r = 190$ with the Boltzmann constant k_B.

The s- and p-wave scattering lengths for ultracold collisions in fermionic ytterbium are measured to be $a = -25a_0$, $b_{\uparrow\downarrow} = -74a_0$, $b_{\uparrow\uparrow}^3 = 0.1b_{\uparrow\downarrow}^3$, and $b_{\downarrow\downarrow} \approx 0$ with the Bohr radius a_0.[38] Additionally, it has been experimentally verified that p-wave interactions between on-site atoms predominate collisional frequency shifts in ytterbium lattice clocks. In contrast, the s-wave scattering may be ruled out even in the presence of large excitation inhomogeneity. Thus, here we only take into account collisions between atoms on the same lattice site.

Besides atom–atom collisions, various technical defects may also affect the resolution of the gravitational redshift detection. The temperature gradient varies the BBR shift across the atomic sample. According to the recent experiment,[15] this BBR shift inhomogeneity is negligible across a 1-mm sample at room temperature and the relevant uncertainty can be bound to the 10^{-21} level. Although two clocks (subensembles) are located in the same optical lattice, the lattice beam inhomogeneity can cause the light shift gradient across the atomic sample, which is estimated to be at the 10^{-21} mm^{-1} level. In addition, the magnetic field gradient induced by nearby magnetic materials introduces the inhomogeneous Zeeman shift across the atomic sample. The first-order Zeeman shifts can be canceled by averaging the frequency between the two $6s\ {}^1S_0(F = 1/2, M_F = \pm 1/2) - 6p\ {}^3P_0(F = 1/2, M_F = \pm 1/2)$ clock transitions. The *in-situ* frequency imaging of lattice-trapped sample[29] enables the measurement of the local stray magnetic field across the entire sample and further allows for the correction of the second-order Zeeman shifts. According to recent experimental conditions,[15] the Zeeman shift inhomogeneity across a 1-mm sample can be controlled at the 10^{-19} level. Nevertheless, the frequency shifts caused by technical defects are not the main focus of this work. These technical defects may be addressed by future new techniques.

We perform the simulation of the clock operation as follows: (i) In each clock cycle, the number n_m of atoms on the mth lattice site is numerically generated following Eq. (3) under the condition $N = \sum_m n_m$. (ii) The radial motional

states $\phi_{m_x}(x)$ and $\phi_{m_y}(y)$ for atoms are created according to the Fermi–Dirac distribution with the Fermi temperature $T_F = 100$ nK.[14] (iii) The ensemble of atoms is divided into the groups with $m \leq 0$ (clock 1) and $m > 0$ (clock 2). For clock $i = 1,2$, we perform the Ramsey measurement in the presence of atom–atom collisions and derive the fractional population p_i of atoms in $|\uparrow\rangle$. (iv) The differential frequency between the two clocks is evaluated by

$$\delta\nu = \frac{p_2 - p_1}{2\pi T_{\rm dark}}. \tag{16}$$

More details on the numerical simulation can be found in Appendix A.

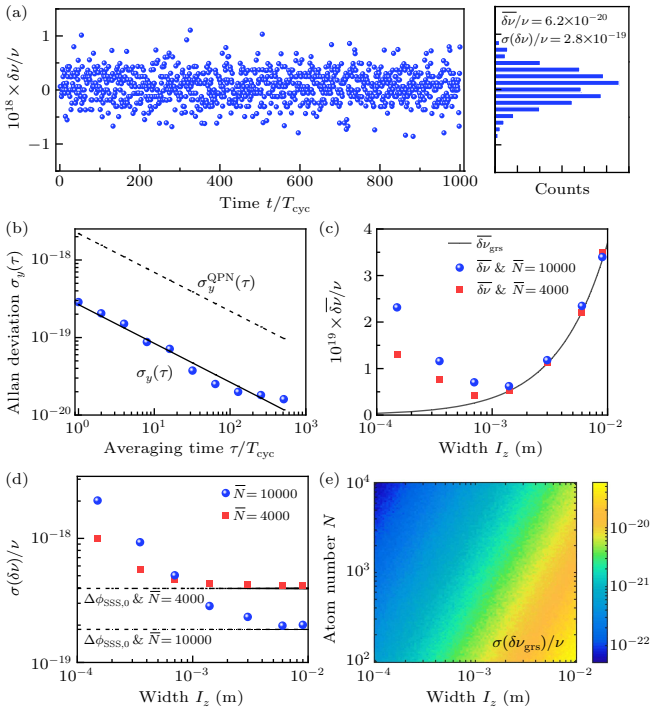


Fig. 3. Simulation of differential frequency comparison between two clocks within one atomic cloud. (a) Fractional frequency difference $(\delta\nu/\nu)$ as a function of time t (in units of the clock cycle duration $T_{\rm cyc}$). The atomic cloud size is set to be $l_z = 1.4$ mm. The histogram has a mean value $\overline{\delta\nu} = 0.03$ mHz and a standard deviation $\sigma(\delta\nu) = 0.15$ mHz. The average and deviation of the atom number are $\bar{N} = 10^4$ and $\sigma_N = 10^2$, respectively. The corresponding Allan deviation $\sigma_y(\tau)$ is shown in panel (b), where τ denotes the sampling time. Symbols: numerical results. Solid curve: curve fitting, $\sigma_y(\tau) = 2.8\times10^{-19}\sqrt{T_{\rm cyc}/\tau}$. Dashed line: the corresponding QPN-limited comparison, $\sigma_y^{\rm QPN}(\tau) = 3.1\times10^{-18}\sqrt{T_{\rm cyc}/\tau}$ in the absence of atom–atom collisions $\hat{V} = 0$. (c) Dependence of $(\overline{\delta\nu}/\nu)$ on l_z with $(\bar{N} = 10^4, \sigma_N = 10^2)$ and $(\bar{N} = 4000, \sigma_N = 40)$. Symbols: numerical results. Solid curve: average gravitational redshift (4). (d) Fractional deviation $\sigma(\delta\nu)/\nu$ vs. l_z with $(\bar{N} = 10^4, \sigma_N = 10^2)$ and $(\bar{N} = 4000, \sigma_N = 40)$. The dashed lines denote the SSS-based uncertainty limit in the absence of atom–atom collisions $\hat{V} = 0$. (e) Fractional deviation $\sigma(\delta\nu_{\rm grs})/\nu$ of the gravitational redshift $\delta\nu_{\rm grs}$ as a function of N and l_z. For all plots, the Ramsey dark time is set to be $T_{\rm dark} = 1$ s.

We simulate the clock operation over multiple cycles as shown in Fig. 3(a). The average frequency difference $\overline{\delta\nu}$ of $\delta\nu$ includes the components of differential collisional shift $\overline{\delta\nu}_{\rm col}$ and gravitational redshift $\overline{\delta\nu}_{\rm grs}$. $\overline{\delta\nu}$ is always positive since clock 1 contains more atoms than clock 2 and $\overline{\delta\nu}_{\rm grs} > 0$ [see Eq. (4)]. We define the condition for resolving the gravitational redshift as $(\overline{\delta\nu}_{\rm grs}/\overline{\delta\nu}_{\rm col}) > 1$. The standard deviation $\sigma(\delta\nu)$ of $\delta\nu$ determines the differential frequency stability $\sigma_y(\tau)$. The numerical simulation suggests that $\sigma_y(\tau)$ takes the form (Fig. 3(b))

$$\sigma_y(\tau) = \frac{\sigma(\delta\nu)}{\nu}\sqrt{\frac{T_{\rm cyc}}{\tau}}, \tag{17}$$

that is, the white phase noise dominates the synchronous comparison.

2.5. Resolution of gravitational redshift

We now study resolving the gravitational redshift in the presence of atom–atom collisions. The number of lattice-trapped atoms is chosen to be $\bar{N} = 10^4$. Thus, each clock contains about $\bar{N}_{1,2} = 5000$ atoms. Figure 3(c) shows the dependence of the average differential frequency $\overline{\delta\nu}$ on the sample size l_z. It is seen that $\overline{\delta\nu}$ well matches the analytical gravitational redshift (4), i.e., $\overline{\delta\nu} \approx \overline{\delta\nu}_{\rm grs}$, for a large l_z, indicating the substantial suppression of interatomic interactions. The average on-site atom number may be estimated by $\bar{n} = \bar{N}/N_{\rm L}$ with the number of lattice sites $N_{\rm L} = 2l_z/\lambda_{\rm mag}$ over the sample width l_z. A large l_z (i.e., an extended sample) may reduce $\bar{n}$ to less than unity and, as a result, the on-site collisions between atoms hardly occur. Nonetheless, it should be noted that although $\bar{n} < 1$, the number of atoms on a lattice site may be higher than unity due to the inhomogeneous atomic distribution in the axial direction.

Reducing l_z raises $\bar{n}$, thereby enhancing the collisional shift $\overline{\delta\nu}_{\rm col} = \overline{\delta\nu} - \overline{\delta\nu}_{\rm grs} > 0$. As the sample width goes down to $l_z \approx 1.4$ mm, which yields $\bar{n} = 2.7$, $\overline{\delta\nu}$ starts to deviate from Eq. (4), denoting that the collisional shift exceeds the gravitational redshift, $\overline{\delta\nu}_{\rm col}/\overline{\delta\nu}_{\rm grs} > 1$. Thus, the minimum size of the atomic cloud for resolving the gravitational redshift reaches $\min(l_z) \approx 1.4$ mm, corresponding to a fractional gravitational redshift of $\overline{\delta\nu}_{\rm grs}/\nu = 5.2\times10^{-20}$ and an effective height difference $\Delta z_{\rm eff} = 0.48$ mm between the two clocks. Reducing the atom number N may reduce the minimum resolvable $\Delta z_{\rm eff}$ (Fig. 3(c)). However, as we will see below, a smaller N leads to larger fluctuations of $\delta\nu$, thereby extending the required averaging time for resolving $\Delta z_{\rm eff}$.

The standard deviation $\sigma(\delta\nu)$ measures the average spread of the differential frequency $\delta\nu$ in each clock cycle around $\overline{\delta\nu}$. A small $\sigma(\delta\nu)$ is highly desired due to the shortened measurement time. The numerical results show that $\sigma(\delta\nu) \approx \sqrt{2}\Delta\phi_{\rm SSS,0}/(4\pi T_{\rm dark}\nu) = 1.9\times10^{-19}$ for a large enough sample size l_z, i.e., sufficiently suppressing atom–atom collisions (Fig. 3(d)). That is, the fluctuations of $\delta\nu$ primarily originate from the projection noise that has been reduced using spin squeezing. A smaller N raises $\Delta\phi_{\rm SSS,0}$ and further elevates $\sigma(\delta\nu)$. Indeed, besides the projection noise in Ramsey measurement, two other factors also contribute to $\sigma(\delta\nu)$.

The density distribution of lattice-trapped atoms differs for different clock cycles, leading to the fluctuations of gravitational redshift and collisional shift.

According to Eqs. (1) and (3), one may numerically compute the deviation $\sigma(\delta\nu_{\rm grs})$ of the measured differential gravitational shift $\delta\nu_{\rm grs}$. The simulation results (Fig. 3(e)) illustrate: (i) $\sigma(\delta\nu_{\rm grs})$ goes down as the atom number N is increased and the corresponding scaling is derived as $\sigma(\delta\nu_{\rm grs}) \propto N^{-0.5}$. This can be roughly interpreted as follows: $\delta\nu_{\rm grs}$ mainly results from the atom number difference $\delta N = N_2 - N_1$ between the two clocks. For different clock cycles, δN varies independently of each other, which may be viewed as a Markov process (i.e., white Gaussian fluctuations). The strength (variance) of fluctuations of δN is proportional to N, resulting in the relative standard deviation $\sigma(\delta N)/N \propto N^{-0.5}$ and further $\sigma(\delta\nu_{\rm grs}) \propto N^{-0.5}$. (ii) $\sigma(\delta\nu_{\rm grs})$ goes up as the cloud size l_z is increased and the corresponding scaling is given by $\sigma(\delta\nu_{\rm grs}) \propto N$. This is because the effective height difference $\Delta z_{\rm eff}$ between the two clocks is proportional to l_z. Nonetheless, the numerical results presented in Fig. 3(e) indicate that within the (N, l_z) regime of interest in this work, $\sigma(\delta\nu_{\rm grs})$ is less than 10^{-20}, well below the deviation $\sigma(\delta\nu)$ of the measured differential frequency $\delta\nu$. Thus, the contribution of $\sigma(\delta\nu_{\rm grs})$ to $\sigma(\delta\nu)$ is negligible.

As shown in Fig. 3(d), the deviation $\sigma(\delta\nu)$ grows when l_z becomes shorter. This behavior results from the enhanced degradation of spin squeezing. The increased average number $\bar{n}$ leads to stronger collisions between on-site atoms. It breaks the interatomic phase relation that is essential to spin squeezing and, as a result, the phase uncertainty $\Delta\phi_{\rm SSS}$ (in the presence of atom–atom collisions $\hat{V} \neq 0$) well exceeds $\Delta\phi_{\rm SSS,0}$ (in the absence of atom–atom collisions $\hat{V} = 0$). For the sample width $l_z = 1.4$ mm, the deviation $\sigma(\delta\nu)$ yields the differential frequency stability $\sigma_y(\tau) = (2.8\times10^{-19})\sqrt{T_{\rm cyc}/\tau}$ (Fig. 3(b)). Thus, when the sampling time τ is longer than one hundred times the clock cycle $T_{\rm cyc}$, the statistical uncertainty $\sigma_y(\tau)$ is well below the average fractional gravitational redshift $\overline{\delta\nu_{\rm grs}}/\nu$. For $T_{\rm cyc}$ of the order of 1 s, the gravitational redshift on the sub-millimeter scale may be resolved within hundreds of seconds of averaging. In contrast, the synchronous measurement between two optical clocks with independent atoms has a QPN-limited stability $\sigma_y^{\rm QPN}(\tau) = (3.1\times10^{-18})\sqrt{T_{\rm cyc}/\tau}$ when $\hat{V} = 0$ (Fig. 3(b)). For a given measurement precision, the required averaging time τ can be shortened by a factor of 120 using spin squeezing.

In the recent experiment,[15] 10^5 independent atoms were employed to resolve the gravitational redshift across a millimeter-scale atomic sample and the resultant stability of the differential frequency comparison reached $\sigma_y(\tau) = 4.8\times10^{-18}/\sqrt{\tau}$. The sufficient suppression of the statistical uncertainty requires the measurement time to exceed 1 hour. By contrast, in our work the total number of lattice-trapped atoms is ten times smaller than that of Ref. [15] and the resolvable height difference is less than half a millimeter within an averaging time of hundreds of seconds, showing the advantages of spin squeezing.

3. Discussion

We have numerically studied the spin-squeezing-enhanced differential frequency comparison of two optical clocks within one lattice-trapped cloud of atoms. The atom–atom collisions limit the resolution of the gravitational redshift to less than one half of a millimeter. The corresponding fractional redshift reaches as low as 5.2×10^{-20} with a statistical uncertainty following $\sigma_y(\tau) = (2.8\times10^{-19})/\sqrt{\tau}$ when setting the clock cycle time to be $T_{\rm cyc} \approx 1$ s. Further reducing the resolvable height difference, especially to the microscale, is highly desired since the nature of quantum effects will be manifested. Exploring "how Einstein's theory of relativity affects the quantum behaviors of atoms" is helpful for unifying these two seemingly incompatible theories, namely, the general relativity and quantum mechanics. Recently, relevant theoretical studies have been launched to explore the mass-energy equivalence effects of general relativity on quantum coherence and entanglement through the comparison of OLCs.[39]

The differential frequency comparison can be also performed between two independent optical clocks that are located in separate lattices as shown in Fig. 4(a). Let us first evaluate the fractional collisional shift of one clock. When the height difference between the two clocks is set to be zero $\Delta z = 0$ (i.e., zero differential gravitational shift) and clock 1 is assumed to be an ideal clock with a fractional excitation $p_1 = 0.5$ (i.e., zero collisional shift), the differential frequency $\delta\nu$ equals the collisional shift of clock 2. Figures 4(b) and 4(c) illustrate that for an atomic cloud size exceeding 1 mm, the fractional collisional shift of the clock transition can be lower than 10^{-20} and the statistical uncertainty is at the low 10^{-19} level, similar to that of the differential frequency comparison of two clocks (sub-ensembles) within one atomic cloud. Nonetheless, the environmental noise perturbs two clocks independently and cannot be rejected in the differential frequency comparison. The major noise source arises from the lattice-induced light shift of the clock transition[11,40,41]

$$\begin{aligned} h\delta\nu_{\rm LS}(u,\delta_{\rm L}) =\ & (1/2)(\delta_{\rm L}\partial_\nu\tilde{\alpha}^{\rm E1} - \tilde{\alpha}^{\rm qm})u^{1/2} \\ & -(\delta_{\rm L}\partial_\nu\tilde{\alpha}^{\rm E1} + 3\tilde{\beta}/4)u + \tilde{\beta}u^{3/2} - \tilde{\beta}u^2, \quad (18) \end{aligned}$$

where $u = U/E_{\rm rec}$, $\delta_{\rm L}$ denotes the detuning of the lattice laser with respect to the magic wavelength $\lambda_{\rm mag}$, and $\partial_\nu\tilde{\alpha}^{\rm E1}/h = 25.74$ μHz/MHz, $\tilde{\alpha}^{\rm qm}/h = -1027$ μHz, and $\tilde{\beta}/h = -1.194$ μHz respectively correspond to the frequency derivative of the differential electric dipole (E1) polarizability,

the differential multipolar polarizability, and the differential hyperpolarizability between $|\uparrow\rangle$ and $|\downarrow\rangle$. Here, we have assumed that all atoms are in the lowest Wannier–Stark state on each lattice site. Substituting $u = 10$, one finds $\delta_{\rm L} = 1.3$ MHz for the zero light shift $\delta\nu_{\rm LS} = 0$. Controlling the lattice-intensity variation within 10% and narrowing the lattice laser linewidth to 50 kHz can suppress the fractional uncertainty of $\delta\nu_{\rm LS}$ to 1.7×10^{-19}. The other noise source is the BBR shift $\delta\nu_{\rm BBR} = -(1.25\ {\rm Hz})(T/300\ {\rm K})^4$, where T is the ambient temperature and we have omitted the small dynamic contribution.[42] Placing the clocks into the cryogenic environment at $T = 77$ K reduces the fractional BBR shift to 1.7×10^{-18}. The fractional uncertainty of $\delta\nu_{\rm BBR}$ may be controlled at the 10^{-20} level by suppressing the temperature variation down to less than 0.1 K. In addition, the Zeeman shifts of clock transitions also affect the clock comparison. During the clock operation, the first-order Zeeman shift is cancelled through averaging the frequencies of clock transitions with opposite spin states. The second-order Zeeman shift that arises from the bias magnetic field is evaluated by b_2B^2 with $b_2 = -6.10\ {\rm MHz\cdot T^{-2}}$.[8] For a typical bias of $B = 0.5$ G, the second-order Zeeman shift for ^{171}Yb clock transition is -15 mHz and the uncertainty can be controlled below 0.5 mHz.[8] The fractional uncertainty of Zeeman shifts is at the 10^{-19} level. All these systematic uncertainties limit the resolution of the fractional gravitational redshift to the 10^{-18} level, corresponding to a centimeter-scale difference in height.

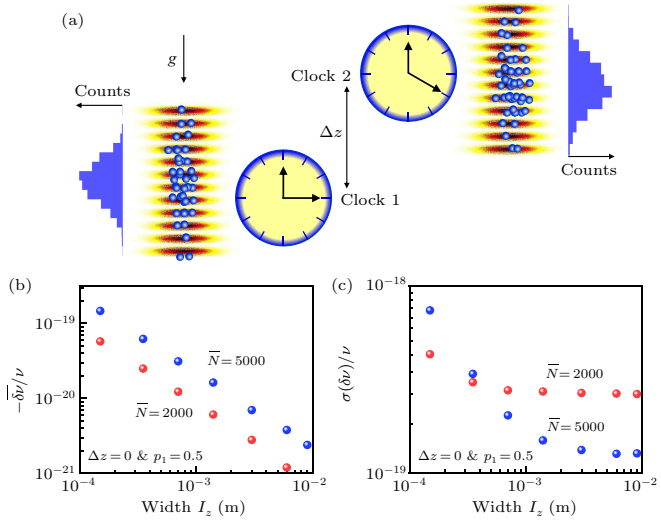


Fig. 4. (a) Differential frequency comparison of two optical clocks that are situated in independent lattices. (b) Average differential frequency $\overline{\delta\nu}$ between the two clocks. Here, the height difference is set to be $\Delta z = 0$ and clock 1 is assumed to be an ideal clock with $p_1 = 0.5$ (i.e., zero collisional shift). In this case, $\overline{\delta\nu}$ equals to the collisional shift of clock 2. The corresponding deviation $\sigma(\delta\nu)$ is shown in panel (c). Two clocks have the same average and deviation of the atom number, $\bar{N} = 5000$ (2000) and $\sigma_N = 50$ (20). The Ramsey dark time is set to be $T_{\rm dark} = 1$ s.

Spin-squeezed lattice clocks have been recently demonstrated in experiments.[23,25] The total phase uncertainty induced by the environmental noise (including lattice-induced light shifts, BBR shifts, and Zeeman shifts) is estimated to be at the 0.1-mrad level for a Ramsey dark period of 1 s. Such a low phase uncertainty hardly affects the degree of spin squeezing. However, in Ref. [23] the Ramsey dark period was limited to 0.17 ms, much shorter than atom–laser and atom–atom coherence times,[15] so as to optimize the degree of spin squeezing. In Ref. [25], the state-of-the-art clock laser, whose coherence time exceeded 10 s, was employed and the Ramsey dark time was only extended to 4 ms. The short dark period strongly limits the phase resolution/sensitivity of the Ramsey spectroscopy. The potential reason for such a short dark period may be the leakage of the anti-squeezed variance into the final spin-population measurement through the clock laser noise.[43,44]

Appendix A: Simulation of synchronous comparison

In each clock cycle, the number of lattice-trapped atoms N is generated according to the normal distribution with the mean $\bar{N}$ and deviation σ_N. N random integers are then created, where the probability of finding the integer m follows the Gaussian function (3) that describes the axial distribution of atoms. n_m is used to denote the number of occurrences of m in the integer array. That is, there are n_m atoms localized on the mth lattice site. In the radial direction, the atoms are distributed over different harmonic oscillators $\phi_{m_x}(x)$ and $\phi_{m_y}(y)$ according to the Fermi–Dirac function

$$F_{m_x,m_y} = \frac{m_x+m_y+1}{{\rm e}^{(m_x+m_y+1)h\nu_{\rm r}/k_{\rm B}T_{\rm r}-T_{\rm F}/T_{\rm r}}+1}, \tag{A1}$$

with the radial indices $m_x \geq 0$ and $m_y \geq 0$ along the x- and y-direction, respectively, the harmonic oscillation frequency $\nu_{\rm r}$, the radial temperature $T_{\rm r}$, and the Fermi temperature $T_{\rm F}$. n_m pairs of random integers (m_x, m_y) are generated following the probability (A1) under the condition that each pair is unique, i.e., Pauli exclusion principle. As a result, each atom is labeled by $\boldsymbol{m} = (m_x, m_y, m)$.

For two clocks within one atomic cloud, the atoms with $m \leq 0$ ($m > 0$) belong to clock 1 (2). Two clocks are treated separately. The Hilbert space for clock $i = 1,2$ is spanned by the Dicke states $\{|S,M\rangle, M = -S,\ldots,S\}$ with $S = N_i/2$. N_i is the number of atoms in clock i and $N_1 + N_2 = N$. For either clock, the SSS-based Ramsey measurement is computed according to Eq. (13). The final state of clock i after the second Ramsey pulse can be written in a superposition form, $\psi = \sum_M c_M |S,M\rangle$. The probability of the projection measurement result in M, i.e., $(S+M)$ atoms in clock i are in $|\uparrow\rangle$, is given by $f_M = |c_M|^2$. A certain $(S+M)$ should be selected as the Ramsey measurement result in a clock cycle. The Monte Carlo method is summarized as follows. The elements

in the array $\{f_{-S}, f_{-S+1}, \ldots, f_{S-1}, f_S\}$ are shuffled and a uniform random number ε in $[0,1]$ is created. Then, ε is compared to the first element $f_{\tilde{M}}$ in the shuffled array. If $\varepsilon < (f_{\tilde{M}}/f_{\max})$, the projection measurement result is $(S+\tilde{M})$, leading to the fractional population $p_i = (S+\tilde{M})/2S$ in clock i. Otherwise, the procedure is repeated. Here, $f_{\max}$ denotes the maximum element in the array. Finally, the fractional populations $p_{1,2}$ of two clocks are obtained and the differential frequency $\delta\nu$ is computed by Eq. (16).

Acknowledgments

Project supported by CAS Project for Young Scientists in Basic Research (Grant No. YSBR-085), the National Time Service Center (Grant No. E239SC1101), Innovation Program for Quantum Science and Technology (Grant No. 2021ZD0303200), and China Postdoctoral Science Foundation (Grant No. BX2021020).

References

[1] Pound R V and Rebka G A 1960 *Phys. Rev. Lett.* **4** 337
[2] Pound R V and Snider J L 1964 *Phys. Rev. Lett.* **13** 539
[3] Pound R V and Snider J L 1965 *Phys. Rev. Lett.* **140** BB788
[4] Vessot R F C, Levine M W, Mattison E M, Blomberg E L, Hoffman T E, Nystrom G U, Farrel B F, Decher R, Eby P B, Baugher C R, Watts J W, Teuber D L and Wills F D 1980 *Phys. Rev. Lett.* **45** 2081
[5] Smarr L L, Vessot R F C, Lundquist C A, Decher R and Piran T 1983 *Gen. Relat. Gravit.* **15** 129
[6] Delva P, Puchades N, Schönemann E, Dilssner F, Courde C, Bertone S, Gonzalez F, Hees A, Le Poncin-Lafitte Ch, Meynadier F, Prieto-Cerdeira R, Sohet B, Ventura-Traveset J and Wolf P 2018 *Phys. Rev. Lett.* **121** 231101
[7] Takano T, Takamoto M, Ushijima I, Ohmae N, Akatsuka T, Yamaguchi A, Kuroishi Y, Munekane H, Miyahara B and Katori H 2016 *Nat. Photon.* **10** 662
[8] McGrew W F, Zhang X, Fasano R J, Schäffer S A, Beloy K, Nicolodi D, Brown R C, Hinkley N, Milani G, Schioppo M, Yoon T H and Ludlow A D 2018 *Nature* **564** 87
[9] Takamoto M, Ushijima I, Ohmae N, Yahagi T, Kokado K, Shinkai H and Katori H 2020 *Nat. Photon.* **14** 411
[10] Bloom B J, Nicholson T L, Williams J R, Campbell S L, Bishof M, Zhang X, Zhang W, Bromley S L and Ye J 2014 *Nature* **506** 71
[11] Ushijima I, Takamoto M and Katori H 2018 *Phys. Rev. Lett.* **121** 263202
[12] Kim K, Aeppli A, Bothwell T and Ye J 2023 *Phys. Rev. Lett.* **130** 113203
[13] Ushijima I, Takamoto M, Das M, Ohkubo T and Katori H 2015 *Nat. Photon.* **9** 185
[14] Aeppli A, Chu A, Bothwell T, Kennedy C J, Kedar D, He, P, Rey A M and Ye J 2022 *Sci. Adv.* **8** eadc9242
[15] Bothwell T, Kennedy C J, Aeppli A, Kedar D, Robinson J M, Oelker E, Staron A and Ye J 2022 *Nature* **602** 420
[16] Santarelli G, Audoin C, Makdissi A, Lauren P, Dick G J and Clairon A 1998 *IEEE Trans. Ultrason. Ferroelectr. Freq. Control* **45** 887
[17] Takamoto M, Takano T and Katori H 2011 *Nat. Photon.* **5** 288
[18] Itano W M, Bergquist J C, Bollinger J J, Gilligan J M, Heinzen D J, Moore F L, Raizen M G and Wineland D J 1993 *Phys. Rev. A* **47** 3554
[19] Santarelli G, Laurent Ph, Lemonde P, Clairon A, Mann A G, Chang S, Luiten A N and Salomon C 1999 *Phys. Rev. Lett.* **82** 4619
[20] Wineland D J, Bollinger J J, Itano W M, Moore F L and Heinzen D J 1992 *Phys. Rev. A* **46** R6797
[21] Kitagawa M and Ueda M 1993 *Phys. Rev. A* **47** 5138
[22] Ma J, Wang X, Sun C P and Nori F 2011 *Phys. Rep.* **509** 89
[23] Pedrozo-Peñafiel E, Colombo S, Shu C, Adiyatullin A F, Li Z, Mendez E, Braverman B, Kawasaki A, Akamatsu D, Xiao Y and Vuletić V 2020 *Nature* **588** 414
[24] Schleier-Smith M H, Leroux I D and Vuletić V 2010 *Phys. Rev. A* **81** 021804
[25] Robinson J M, Miklos M, Tso Y M, Kennedy C J, Bothwell T, Kedar D, Thompso J K and Ye J 2024 *Nat. Phys.* **20** 208
[26] Chen J and Yu D 2024 *Sci. Bull.* **69** 1359
[27] Lemonde P and Wolf P 2005 *Phys. Rev. A* **72** 033409
[28] Yu D 2012 *Phys. Rev. A* **85** 032705
[29] Marti G E, Hutson R B, Goban A, Campbell S L, Poli N and Ye J 2018 *Phys. Rev. Lett.* **120** 103201
[30] Yu D, Chen J and Zhang S 2023 *Phys. Rev. A* **107** 043120
[31] Dörscher S, Schwarz R, Al-Masoudi A, Falke S, Sterr U and Lisdat C 2018 *Phys. Rev. A* **97** 063419
[32] Wang C, Yao Y, Shi H, Yu H, Ma L and Jiang Y 2024 *Chin. Phys. B* **33** 030601
[33] Porsev S G, Derevianko A and Fortson E N 2004 *Phys. Rev. A* **69** 021403
[34] Hutson R B, Goban A, Marti G E, Sonderhouse L, Sanner C and Ye J 2019 *Phys. Rev. Lett.* **123** 123401
[35] Yu D, Zhang J, Xia T, Zhang S, Shi T and Chen J 2024 *Phys. Rev. A* **110** 013102
[36] Zhang X, Beloy K, Hassan Y S, McGrew W F, Chen C C, Siegel J L, Grogan T and Ludlow A D 2022 *Phys. Rev. Lett.* **129** 113202
[37] Siegel J L, McGrew W F, Hassan Y S, Chen C C, Beloy K, Grogan T, Zhang X and Ludlow A D 2024 *Phys. Rev. Lett.* **132** 133201
[38] Lemke N D, von Stecher J, Sherman J A, Rey A M, Oates C W and Ludlow A D 2011 *Phys. Rev. Lett.* **107** 103902
[39] Chu A, Martínez-Lahuerta V J, Miklos M, Kim K, Zoller P, Hammerer K, Ye J and Rey A M 2025 *Phys. Rev. Lett.* **134** 093201
[40] Ovsiannikov V D, Marmo S I, Palchikov V G and Katori H 2016 *Phys. Rev. A* **93** 043420
[41] Nemitz N A, Jørgensen A, Yanagimoto R, Bregolin F and Katori H 2019 *Phys. Rev. A* **99** 033424
[42] Sherman J A, Lemke N D, Hinkley N, Pizzocaro M, Fox R W, Ludlow A D and Oates C W 2012 *Phys. Rev. Lett.* **108** 153002
[43] Braverman B, Kawasaki A and Vuletić V 2018 *New J. Phys.* **20** 103019
[44] Caprotti A, Barbiero M, Tarallo M G, Genoni M G and Bertaina G 2024 *Quantum Sci. Technol.* **9** 035032